Magneto-optical effects in multilayers illuminated by total internal reflection

N. Richard, A. Dereux, T. David, E. Bourillot, and J. P. Goudonnet

Laboratoire de Physique, Optique Submicronique, Université de Bourgogne, BP400, 21011 Dijon, France

F. Scheurer, E. Beaurepaire, and G. Garreau

Institut de Physique et Chimie des Matériaux de Strasbourg, 23 Rue du Loess, Boîte Postale 20 CR, 67037 Strasbourg, France

(Received 24 June 1998)

This paper describes the magneto-optical effects of metallic multilayers under the condition of total internal reflection. In the framework of Green's dyadic technique, we detail a practical and at time-consuming scheme to compute accurately the optical properties of anisotropic multilayers deposited on a substrate. We present numerical simulations which account for the variation of the angle of incidence at a fixed wavelength and for the variation of the wavelength at fixed angle of incidence. The Kerr rotation is found to increase significantly around the critical angle for total reflection. We also discuss the importance of plasmon effects in the structure of the Kerr rotation spectra. [S0163-1829(99)00708-0]

I. INTRODUCTION

The magneto-optical Kerr effect has become an important magnetic characterization technique in the field of magnetic ultrathin films and multilayers, and is also used in optical reading devices.[1,2] Most studies consider the Kerr effect in external illumination by varying the angle of incidence and/or the thickness of the magneto-optical thin films.[3,4] Other experiments investigate the variation of the incident photon energy at a fixed angle of incidence.[5,6] Recent works study the Kerr effect of multilayers made of magnetic materials by illuminating through a transparent substrate at a fixed angle of incidence and as a function of the wavelength,[7,8] or at fixed wavelength as a function of the angle of incidence.[9] These last papers have brought to the fore the role of surface plasmons in the magneto-optical signal.

In this paper, we analyze accurately the variations of the reflectivity and the magneto-optical Kerr rotation module as a function of the angle of incidence from a theoretical point of view. We underline the role of resonance phenomena in the multilayer structure. This resonance occurs at an angle close to the critical angle for total reflection and/or when a surface plasmon is excited. The numerical method used for these calculations is based on the Green's dyadic technique,[10] which is introduced below. We focus our study on the Kerr effect of magneto-optical thin films deposited on a glass substrate. The films are illuminated through the substrate beyond the critical angle for total internal reflection. The two polarization modes TE and TM are considered for the incident electric field associated with the laser beam. In the TE mode, the incident electric field is perpendicular to the plane of incidence (the so-called *s* polarization), whereas this field is parallel to it in the TM mode (the *p* polarization).

The reflectivity and the Kerr rotation module are computed as a function of the angle of incidence in the far field. This study will also be done at a fixed angle as a function of the incident wavelength in order to simulate a spectroscopy experiment.

In Sec. II, we will describe the principles of the method used for computing the optical properties and the magneto-optical effects. Section III recalls the anisotropic aspect of magnetic films. Section IV shows numerical results obtained on bilayers composed of a nonmagnetic material (Au) and a magnetic material (Co).

II. OPTICAL PROPERTIES OF AN ANISOTROPIC MULTILAYER SYSTEM

A. Scattering theory

Our theoretical analysis of the propagation of electromagnetic fields through an arbitrary anisotropic multilayered structure is based on scattering theory. In this theory, one describes the scattering of waves relatively to a reference system. In the context of multilayers, it is convenient to choose such a system as the single surface geometry made of two semi-infinite isotropic media.[11] Let $\varepsilon_1(z,\omega)$ be the frequency (ω)-dependent dielectric function profile of this surface system.

Assuming that the fields have an harmonic time dependence $e^{-i\omega t}$ in Maxwell's equations, the vectorial wave equation satisfied by the electric field is (c is the speed of light in vacuum):

$$-\vec{\nabla}\times\vec{\nabla}\times\vec{E}(\vec{r})+\frac{\omega^2}{c^2}\varepsilon_1(z,\omega)\vec{E}(\vec{r})=\vec{V}(z,\omega)\vec{E}(\vec{r}). \quad (1)$$

For $z>0$, $\varepsilon_1(z,\omega)$ corresponds to the dielectric function of the external medium:

$$\varepsilon_1(z,\omega)=\varepsilon_a(\omega),$$

while, for $z<0$, $\varepsilon_1(z,\omega)$ is given by the dielectric function of the substrate:

$$\varepsilon_1(z,\omega)=\varepsilon_{sub}(\omega).$$

The perturbation dyadic $\overleftrightarrow{V}(z,\omega)$ is defined by (Fig. 1)

$$\overleftrightarrow{V}(z,\omega)=\frac{\omega^2}{c^2}[\overleftrightarrow{1}\varepsilon_a(\omega)-\overleftrightarrow{\varepsilon}(z,\omega)] \quad (z>0), \quad (2)$$
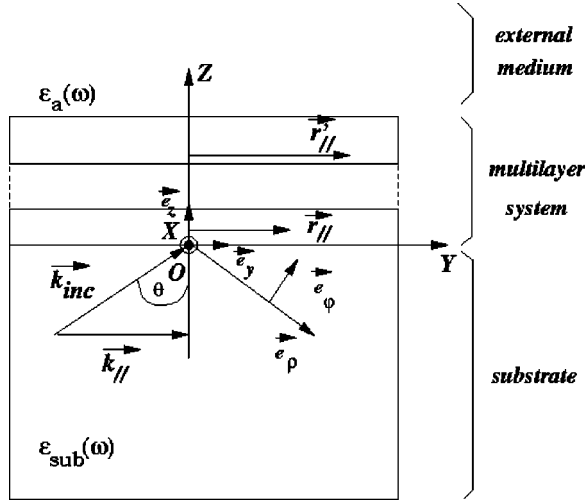
FIG. 1. Geometry of the system. We define $\vec{r}=\vec{r}_{\|}+z\vec{e}_z$, $\vec{r}'=\vec{r}'_{\|}+z'\vec{e}_z$, and $\vec{k}=\vec{k}_{\|}+k_z\vec{e}_z$, and the cylindrical coordinates $(\vec{e}_x,\ \vec{e}_\rho,\ \vec{e}_\phi)$ are used to define the Kerr effect. The radial coordinate $\vec{e}_\rho$ is aligned along the reflected wave vector.

$$\overleftrightarrow{V}(z,\omega)=0 \quad (z<0). \tag{3}$$

$\overleftrightarrow{\varepsilon}(z,\omega)$ is the dielectric tensor of the multilayered structure which is located in the *upper z* plane ($z'>0$). The structure of this tensor is not limited to magneto-optical materials. It can account for any kind of linear anisotropy.

The solution of the scattering problem is given by the Lippmann-Schwinger equation

$$\vec{E}(\vec{r})=\vec{E}^0(\vec{r})+\vec{E}^s(\vec{r}), \tag{4}$$

where $\vec{E}^0(\vec{r})$ and $\vec{E}^s(\vec{r})$ are the incident and the scattered field. The scattered field is given by [A is the domain where $\overleftrightarrow{V}(z',\omega)\neq0$]

$$\vec{E}^s(\vec{r})=\int_A d\vec{r}'\overleftrightarrow{G}(\vec{r},\vec{r}';\omega)\overleftrightarrow{V}(z',\omega)\vec{E}(\vec{r}'). \tag{5}$$

In this last equation, $\overleftrightarrow{G}(\vec{r},\vec{r}';\omega)$ is the Green's dyadic defined by [$\delta(\vec{r}-\vec{r}')$ is the Dirac delta function]

$$-\vec{\nabla}\times\vec{\nabla}\times\overleftrightarrow{G}(\vec{r},\vec{r}';\omega)+\frac{\omega^2}{c^2}\varepsilon_1(z,\omega)\overleftrightarrow{G}(\vec{r},\vec{r}';\omega)=\overleftrightarrow{1}\delta(\vec{r}-\vec{r}'). \tag{6}$$

The planar symmetry of multilayered structures allows to introduce the following Fourier expansions for the fields and the propagator involved in Eqs. (4), (5), and (6):

$$\vec{E}(\vec{r})=\frac{1}{4\pi^2}\int d\vec{k}_{\|}\vec{F}(z;\vec{k}_{\|})e^{i\vec{k}_{\|}\cdot\vec{r}_{\|}}, \tag{7}$$

$$\vec{E}_0(\vec{r})=\frac{1}{4\pi^2}\int d\vec{k}_{\|}\vec{F}_0(z;\vec{k}_{\|})e^{i\vec{k}_{\|}\cdot\vec{r}_{\|}}, \tag{8}$$

$$\overleftrightarrow{G}(\vec{r},\vec{r}';\omega)=\frac{1}{4\pi^2}\int d\vec{k}_{\|}e^{i\vec{k}_{\|}\cdot(\vec{r}_{\|}-\vec{r}'_{\|})}\overleftrightarrow{g}(z,z';\vec{k}_{\|}). \tag{9}$$

The introduction of the Fourier transforms (7)–(9) in Eq. (4) leads to a one-dimensional vector Lippmann-Schwinger equation:

$$\vec{F}(z;\vec{k}_{\|})=\vec{F}_0(z;\vec{k}_{\|})+\int_A dz'\overleftrightarrow{g}(z,z';\vec{k}_{\|})\overleftrightarrow{V}(z',\omega)\vec{F}(z';\vec{k}_{\|}). \tag{10}$$

The numerical analysis is based on the discretization of this last Lippmann-Schwinger equation.[10]

The source coordinate z' being positive, for $z>0$, the dyadic $\overleftrightarrow{g}(z,z';\vec{k}_{\|})$ is the sum of the dyadic Green tensor associated with the external medium $\overleftrightarrow{g}_0(z,z';\vec{k}_{\|})$ and the surface response $\overleftrightarrow{g}_s(z,z';\vec{k}_{\|})$:

$$\overleftrightarrow{g}(z,z';\vec{k}_{\|})=\overleftrightarrow{g}_0(z,z';\vec{k}_{\|})+\overleftrightarrow{g}_s(z,z';\vec{k}_{\|}). \tag{11}$$

For $z<0$, the dyadic is reduced to one term:

$$\overleftrightarrow{g}(z,z';\vec{k}_{\|})=\overleftrightarrow{g}'_s(z,z';\vec{k}_{\|}). \tag{12}$$

B. Green's dyadic for a surface system

Here we detail the analytical structure of $\overleftrightarrow{g}(z,z';\vec{k}_{\|})$. We first precise the two possible values of the wave-vector component along $\vec{e}_z$ ($k_{\|}^2=k_x^2+k_y^2$):

$$k_a=\sqrt{\frac{\omega^2}{c^2}\varepsilon_a-k_{\|}^2}, \tag{13}$$

$$k_{\text{sub}}=\sqrt{\frac{\omega^2}{c^2}\varepsilon_{\text{sub}}-k_{\|}^2}. \tag{14}$$

In the case where $z>0$ and $z'>0$, we find, for $\overleftrightarrow{g}_s(z,z';\vec{k}_{\|})$,

$$\overleftrightarrow{g}_0(z,z';\vec{k}_{\|})=\frac{e^{ik_a|z-z'|}}{2ik_a}\left(\overleftrightarrow{1}-\frac{c^2}{\omega^2\varepsilon_a}\overleftrightarrow{Q}\right)+\frac{c^2}{\omega^2\varepsilon_a}\overleftrightarrow{L}\delta(z-z'), \tag{15}$$

with

$$\overleftrightarrow{Q}=\begin{pmatrix} k_x^2 & k_xk_y & \dfrac{|z-z'|}{z-z'}k_xk_a \\[2ex] k_xk_y & k_y^2 & \dfrac{|z-z'|}{z-z'}k_yk_a \\[2ex] \dfrac{|z-z'|}{z-z'}k_xk_a & \dfrac{|z-z'|}{z-z'}k_yk_a & k_a^2 \end{pmatrix}. \tag{16}$$

The tensor

$$\overleftrightarrow{L}=\begin{pmatrix} 0 & 0 & 0 \\ 0 & 0 & 0 \\ 0 & 0 & 1 \end{pmatrix} \tag{17}$$

accounts for the depolarization of a discretized cell which has the shape of a very thin film.[12] The dyadic $\overleftrightarrow{g}_s(z,z';\vec{k}_{\|})$ describing the surface response when $z>0$ is

$$\overleftrightarrow{g}_s(z,z';\vec{k}_\parallel)$$

$$=\frac{1}{k_\parallel^2}\begin{pmatrix} k_x^2 D_{xx}+k_y^2 D_{yy} & k_x k_y(D_{xx}-D_{yy}) & k_\parallel k_x D_{xz} \\ k_x k_y(D_{xx}-D_{yy}) & k_y^2 D_{xx}+k_x^2 D_{yy} & k_\parallel k_y D_{xz} \\ k_\parallel k_x D_{zx} & k_\parallel k_y D_{zx} & k_\parallel^2 D_{zz} \end{pmatrix},$$

(18)

where

$$D_{xx}=-\frac{c^2}{\omega^2\varepsilon_a}k_a^2\frac{k_a\varepsilon_{sub}-k_{sub}\varepsilon_a}{k_a\varepsilon_{sub}+k_{sub}\varepsilon_a}\frac{e^{ik_a(z+z')}}{2ik_a},$$

(19)

$$D_{yy}=\frac{k_a-k_{sub}}{k_a+k_{sub}}\frac{e^{ik_a(z+z')}}{2ik_a},$$

(20)

$$D_{zx}=\frac{c^2}{\omega^2\varepsilon_a}k_a k_\parallel\frac{k_a\varepsilon_{sub}-k_{sub}\varepsilon_a}{k_a\varepsilon_{sub}+k_{sub}\varepsilon_a}\frac{e^{ik_a(z+z')}}{2ik_a},$$

(21)

$$D_{xz}=-\frac{c^2}{\omega^2\varepsilon_a}k_a k_\parallel\frac{k_a\varepsilon_{sub}-k_{sub}\varepsilon_a}{k_a\varepsilon_{sub}+k_{sub}\varepsilon_a}\frac{e^{ik_a(z+z')}}{2ik_a},$$

(22)

$$D_{zz}=\frac{c^2}{\omega^2\varepsilon_a}k_\parallel^2\frac{k_a\varepsilon_{sub}-k_{sub}\varepsilon_a}{k_a\varepsilon_{sub}+k_{sub}\varepsilon_a}\frac{e^{ik_a(z+z')}}{2ik_a}.$$

(23)

For $z<0$ and $z'>0$, the dyadic $\overleftrightarrow{g}(z,z';\vec{k}_\parallel)$ is only due to the response of the surface $\overleftrightarrow{g}_s'(z,z';\vec{k}_\parallel)$ which has the same structure as Eq. (18) but with the following coefficients:

$$D_{xx}=-i\frac{c^2}{\omega^2}\frac{k_a k_{sub}}{k_a\varepsilon_{sub}+k_{sub}\varepsilon_a}e^{ik_a z'-ik_{sub}z},$$

(24)

$$D_{yy}=-\frac{i}{k_a+k_{sub}}e^{ik_a z'-ik_{sub}z},$$

(25)

$$D_{zx}=-i\frac{c^2}{\omega^2}\frac{k_a k_\parallel}{k_a\varepsilon_{sub}+k_{sub}\varepsilon_a}e^{ik_a z'-ik_{sub}z},$$

(26)

$$D_{xz}=-i\frac{c^2}{\omega^2}\frac{k_{sub}k_\parallel}{k_a\varepsilon_{sub}+k_{sub}\varepsilon_a}e^{ik_a z'-ik_{sub}z},$$

(27)

$$D_{zz}=-i\frac{c^2}{\omega^2}\frac{k_\parallel^2}{k_a\varepsilon_{sub}+k_{sub}\varepsilon_a}e^{ik_a z'-ik_{sub}z}.$$

(28)

C. Far-field properties

Considering the reflected electric field in the far field allows some analytical simplifications. In the case of illumination through the substrate, the reflected field reads ($z<0$)

$$\vec{E}_r(\vec{r})=\frac{1}{4\pi^2}\int d\vec{k}_\parallel \vec{f}_r(\vec{k}_\parallel)e^{i\vec{k}_\parallel\cdot\vec{r}_\parallel}e^{-ik_{sub}z},$$

(29)

where

$$\vec{f}_r(\vec{k}_\parallel)=\int_A dz'\,\overleftrightarrow{g}_s'(0,z';\vec{k}_\parallel)\overleftrightarrow{V}(z',\omega)\vec{F}(z';\vec{k}_\parallel).$$

(30)

The transmitted field is then given by ($z>0$)

$$\vec{E}_t(\vec{r})=\frac{1}{4\pi^2}\int d\vec{k}_\parallel \vec{f}_t(\vec{k}_\parallel)e^{i\vec{k}_\parallel\cdot\vec{r}_\parallel}e^{ik_a z},$$

(31)

where

$$\vec{f}_t(\vec{k}_\parallel)=\int_A dz'[\overleftrightarrow{g}_0(0,z';\vec{k}_\parallel)+\overleftrightarrow{g}_s(0,z';\vec{k}_\parallel)]\overleftrightarrow{V}(z',\omega)\vec{F}(z';\vec{k}_\parallel).$$

(32)

In the simple case where the incident field has the form of a plane wave, we have, of course,

$$\vec{F}_0(z;\vec{k}_\parallel)=\vec{A}e^{ik_{sub}z}\delta(\vec{q}_\parallel-\vec{k}_\parallel)+\vec{A}_1 e^{-ik_{sub}z}\delta(\vec{q}_\parallel-\vec{k}_\parallel)\quad(z<0),$$

(33)

$$\vec{F}_0(z;\vec{k}_\parallel)=\vec{A}_2 e^{ik_a z}\delta(\vec{q}_\parallel-\vec{k}_\parallel)\quad(z>0),$$

(34)

where we normalize the TE mode according to

$$\vec{A}=\vec{e}_x,$$

(35)

$$\vec{A}_1=\frac{k_{sub}-k_a}{k_{sub}+k_a}\vec{e}_x,$$

(36)

$$\vec{A}_2=\frac{2k_{sub}}{k_{sub}+k_a}\vec{e}_x,$$

(37)

and the TM mode as follows:

$$\vec{A}=-\cos\theta\vec{e}_y+\sin\theta\vec{e}_z,$$

(38)

$$\vec{A}_1=\frac{k_{sub}\varepsilon_a-k_a\varepsilon_{sub}}{k_{sub}\varepsilon_a+k_a\varepsilon_{sub}}(\cos\theta\vec{e}_y+\sin\theta\vec{e}_z),$$

(39)

$$\vec{A}_2=\frac{2k_{sub}\sqrt{\varepsilon_a}\sqrt{\varepsilon_{sub}}}{k_{sub}\varepsilon_a+k_a\varepsilon_{sub}}(-\cos\theta_t\vec{e}_y+\sin\theta_t\vec{e}_z).$$

(40)

θ is the angle of reflection, θ_t is the angle of transmission, $\vec{q}_\parallel=\sin\theta\vec{e}_y$, and $q=(\omega^2/c^2)\varepsilon_1(z,\omega)$. For the reflection, the scattered field (29) is then reduced to ($z<0$):

$$\vec{E}_r(\vec{r})=\frac{1}{4\pi^2}[\vec{A}_1+\vec{f}_r(\vec{q}_\parallel)]e^{i\vec{q}_\parallel\cdot\vec{r}_\parallel}e^{-ik_{sub}z}.$$

(41)

The reflectivity outside the multilayer then arises as

$$R=\frac{|\vec{A}_1+\vec{f}_r(\vec{q}_\parallel)|^2}{|\vec{A}|^2}.$$

(42)

The transmitted field (31) is also reduced to ($z>0$)

$$\vec{E}_t(\vec{r})=\frac{1}{4\pi^2}[\vec{A}_2+\vec{f}_t(\vec{q}_\parallel)]e^{i\vec{q}_\parallel\cdot\vec{r}_\parallel}e^{ik_a z}.$$

(43)

The normalized transmitted power reads

$$T = \frac{|\vec{A}_2 + \vec{f}_t(\vec{q}_\parallel)|^2}{|\vec{A}|^2} \frac{\text{Re}(k_a)}{\text{Re}(k_{\text{sub}})}. \tag{44}$$

D. Kerr and Faraday effects

The Kerr effect is described by a rotation of the plane of polarization of the reflected field relatively to the incident field. The Faraday effect is the same phenomenon for the transmitted wave. A set of cylindrical coordinates (Fig. 1) based on the reflected wave vector is introduced by

$$f_{r,\rho}(\vec{k}_\parallel) = f_{r,y}(\vec{k}_\parallel)\sin\theta - f_{r,z}(\vec{k}_\parallel)\cos\theta,$$

$$f_{r,\phi}(\vec{k}_\parallel) = f_{r,y}(\vec{k}_\parallel)\cos\theta + f_{r,z}(\vec{k}_\parallel)\sin\theta,$$

$$f_{r,x}(\vec{k}_\parallel) = f_{r,x}(\vec{k}_\parallel). \tag{45}$$

The Kerr rotations Φ'_s and Φ'_p and the ellipticities Φ''_s and Φ''_p correspond to the real and imaginary part of the following ratios:

$$\Phi_s = \frac{f_{r,\phi}(\vec{k}_\parallel)}{f_{r,x}(\vec{k}_\parallel)} = \Phi'_s + i\Phi''_s \quad \text{(TE)}, \tag{46}$$

$$\Phi_p = \frac{f_{r,x}(\vec{k}_\parallel)}{f_{r,\phi}(\vec{k}_\parallel)} = \Phi'_p + i\Phi''_p \quad \text{(TM)}. \tag{47}$$

Similarly, the Faraday effect in the transmitted field is described by using a set of cylindrical coordinates based on the transmitted wave vector in the $\varepsilon_a(\omega)$ medium:

$$f_{t,\rho}(\vec{k}_\parallel) = f_{t,y}(\vec{k}_\parallel)\sin\theta_t + f_{t,z}(\vec{k}_\parallel)\cos\theta_t,$$

$$f_{t,\phi}(\vec{k}_\parallel) = -f_{t,y}(\vec{k}_\parallel)\cos\theta_t + f_{t,z}(\vec{k}_\parallel)\sin\theta_t,$$

$$f_{t,x}(\vec{k}_\parallel) = f_{t,x}(\vec{k}_\parallel). \tag{48}$$

The Faraday rotations β'_s and β'_p and the Faraday ellipticities β''_s and β''_p are defined by

$$\beta_s = \frac{f_{t,\phi}(\vec{k}_\parallel)}{f_{t,x}(\vec{k}_\parallel)} = \beta'_s + i\beta''_s \quad \text{(TE)}, \tag{49}$$

$$\beta_p = \frac{f_{t,x}(\vec{k}_\parallel)}{f_{t,\phi}(\vec{k}_\parallel)} = \beta'_p + i\beta''_p \quad \text{(TM)}. \tag{50}$$

III. MAGNETO-OPTICAL TENSORS

In the case of magnetic materials, the dielectric function is actually a nondiagonal tensor. For ultrathin films or multilayers, the magnetization vector may have components perpendicular to the film plane (so-called polar component) and in this plane (so-called longitudinal component). Here, for simplicity, we will consider pure polar or longitudinal configurations, and we therefore assume that the films are uniformly magnetized. The films must be in a magnetic single-domain state. This can sometimes be obtained in a remanent state or by saturating the films by applying an external static magnetic field (perpendicular or parallel to the film plane).
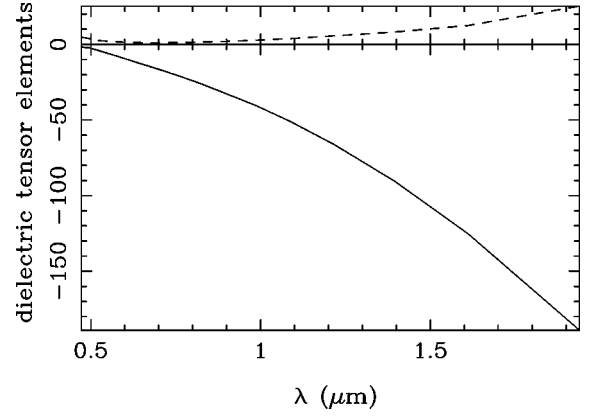

FIG. 2. Variation of the Au dielectric tensor elements as a function of the incident wavelength [solid line: $\text{Re}(\alpha)$; dashed line: $\text{Im}(\alpha)$].

The structures of the magneto-optical tensors are then described by

$$\varepsilon_{\text{polar}} = \begin{pmatrix} \alpha & \beta & 0 \\ -\beta & \alpha & 0 \\ 0 & 0 & \alpha \end{pmatrix}, \tag{51}$$

$$\varepsilon_{\text{longitudinal}} = \begin{pmatrix} \alpha & 0 & -\beta \\ 0 & \alpha & 0 \\ \beta & 0 & \alpha \end{pmatrix}. \tag{52}$$

The complex coefficient β is smaller than the diagonal terms of the tensor. The nondiagonal elements transform an incident rectilinear polarized wave into elliptic reflected and transmitted waves. In the figures discussed below, the systems are always illuminated through the glass substrate, and we used the optical data of Au and Co in Ref. 13 (Fig. 2) and the magneto-optical coefficients of Co from Refs. 13 and 14, which are cast together with the optical constants in Fig. 3.
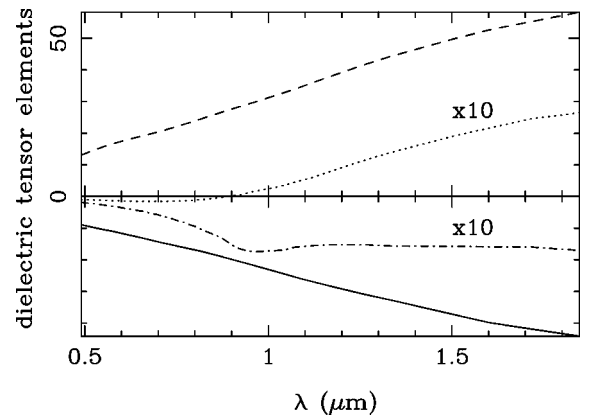

FIG. 3. Variation of the Co dielectric tensor elements as a function of the incident wavelength [solid line: $\text{Re}(\alpha)$; dashed line: $\text{Im}(\alpha)$; dot-dashed line: $\text{Re}(\beta)$ (ten times magnified); dotted line: $\text{Im}(\beta)$ (ten times magnified)].
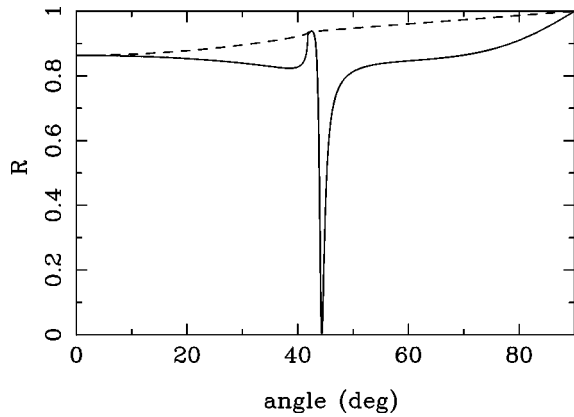
FIG. 4. For $\lambda = 0.633$ μm, reflectivity of a 50-nm-thick Au film deposited on a glass substrate for both TE (dashed line) and TM (solid line) modes, as a function of the angle of incidence. The incident field illuminates the film through the substrate.

IV. NUMERICAL RESULTS

A. Plasmon of a Au thin film

To check the reliability of the numerical technique, we calculate the reflectivity as a function of the angle of incidence of a 50-nm Au layer on a glass substrate. In the calculations, we approximate that the index of refraction of the substrate did not vary as a function of the incident wavelength.

We illuminate the film at $\lambda = 0.633$ μm through the substrate by varying the angle of incidence. This corresponds to the so-called Kretschmann-Raether configuration[15] to excite surface plasmons at the air/gold interface. A plasmon resonance is a surface mode which occurs at a metal/air interface. It depends on the metal film thickness and especially on the absorption of the considered metal. A plasmon resonance of a thin metal film may occur in the Kretschmann-Raether setup if we have the following conditions. First, the incident wave must be TM polarized. Second, the incident wavevector component which is parallel to the interfaces must match the one of the surface plasmon. Third, the metal thickness must be small compared to the incident wavelength to allow the incoming wave to reach the air/gold interface by optical tunneling. This last condition is fulfilled for a 50-nm gold film at $\lambda = 0.633$ μm, and the second condition is satisfied if $\theta = 44.5°$ for which the plasmon excitation frustrates the total reflection and appears as a sharp dip in (Fig. 4). In this figure, we also see a region between the critical angle, corresponding to the total reflection at 41.8°, and 43° where the reflectivity increases (Fig. 4). This narrow peak corresponds to virtual modes which create oscillations of the reflectivity as a function of the metal film thickness, just like a dielectric film would do but without damping: it is the same behavior, just like the interferences in the reflectivity curve in a Perot-Fabry interferometer which displays minima and maxima of the reflectivity as a function of the dielectric film thickness. Indeed, for angles in this peak, if we calculate the reflectivity as a function of the gold thickness, we would find an oscillating exponential decrease of the reflectivity which confirms the presence of these virtual modes which occur within the skin depth of a metal, since the exponential decay is due to the metal absorption.
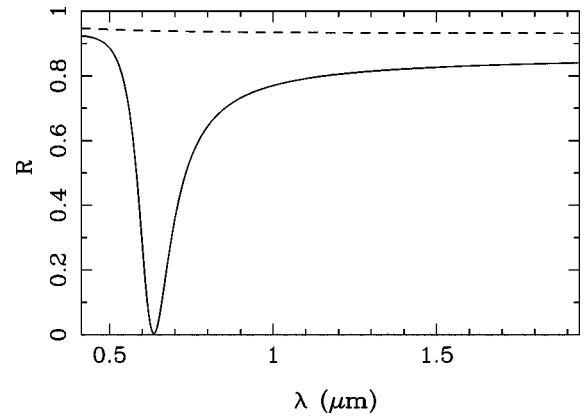

FIG. 5. For the same system as in Fig. 4, and for a $\theta = 44.5°$, variation of the reflectivity for both TE and TM modes as a function of the incident wavelength.

Beyond 43°, we find the well-known plasmon resonance of the gold film occurring at the gold/air interface at 44.5° (Fig. 4). This plasmon resonance can also be seen on the reflectivity curve as a function of the incident wavelength (Fig. 5): it corresponds to a minimum of the reflectivity. The numerical method is thus able to account accurately for well-known phenomena involving isotropic materials.

B. Cobalt

We now apply the numerical scheme to a thin film of Co. Co is a ferromagnetic material which has a great absorption compared to Au. Its plasmon resonance, as a result, must appear for a smaller film thickness.

We set a 13-nm thin film of Co deposited on a glass substrate; this thickness has been chosen in order to obtain the deepest plasmon resonance in the reflectivity curve beyond the critical angle.

In Fig. 6(a), for the TM mode, we recognize the region between 41.8° and 43° corresponding to the virtual modes discussed above for the gold film. The plasmon resonance appears in the reflectivity curve as a function of the angle of incidence at $\theta = 51°$.

We can see at first that when the reflectivity decreases in Fig. 6(a), the Kerr rotation module increases in Fig. 6(b) for both magnetizations of the Co film. This phenomenon is explained by the fact that, when the reflectivity decreases, the light wave goes through the magneto-optical material and, as a result, the Kerr rotation inside the Co layer becomes significant by multiple reflections.

For the TM mode, a peak appears in the Kerr rotation at the plasmon resonance (51°) for both magnetizations. In Fig. 7, between 600 and 750 nm, the plasmon resonance appears as a shoulder to the left of the wavelength 950 nm for which the real part of the magneto-optical coefficient β is extremal in Fig. 5. Because Co has a relatively high absorption, the peak corresponding to the plasmon resonance for Co appears softened in Fig. 7.

For a small Co film thickness, in the polar magnetization, in both TE and TM polarizations, the Kerr rotation module shows a minimum as a function of the angle of incidence just at the critical angle in Fig. 6(b), which is 41.8° for a glass/air interface. For the TM mode, a maximum corresponds to the
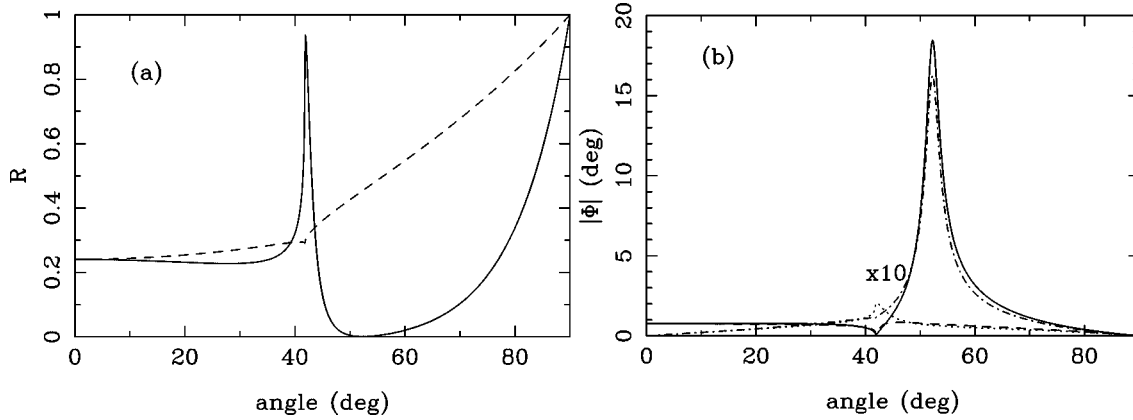
FIG. 6. For $\lambda = 0.633$ μm, (a) reflectivity of a 13-nm-thick Co film on a glass substrate for both TE (dashed line) and TM (solid line) modes as a function of the angle of incidence; (b) variation of the Kerr rotation module $|\Phi|$ of a 13-nm-thick Co film thickness for the TE (dashed line) and TM (solid line) modes for polar magnetization, and for the TE (dotted line) and TM (dot-dashed line) modes for longitudinal magnetization (magnified ten times), as a function of the angle of incidence.

plasmon resonance of Co at 52° [Fig. 6(b)]. For the TE mode, the reflectivity does not show any anomaly, and the Kerr rotation module has a stable behavior as a function of the angle of incidence beyond the critical angle [Fig. 6(b)]. In the longitudinal magnetization, the behaviors are the same as in the polar magnetization, but a slight difference is shown for the TE mode: instead of a dip at the critical angle (41.8°), we have a small increase of the Kerr rotation module [Fig. 6(b)].

We can notice a different order of magnitude in the intensity ranges of the Kerr rotation module for both polar and longitudinal magnetizations. The Kerr rotation module is more important for the polar magnetization as compared to the longitudinal case. This phenomenon is explained by the fact that when a magnetic static field is applied on the electrons, they are submitted to the Laplace force $-e\vec{v}_e \times \vec{B}_0$, where $-e$ is the charge of an electron, $\vec{v}_e$ its speed, and $\vec{B}_0$ the applied magnetic field. This force creates the rotation for the electrons. As a result, the electrons motion is constrained by the film thickness in the longitudinal case, whereas it is not for the polar case: the electrons can move
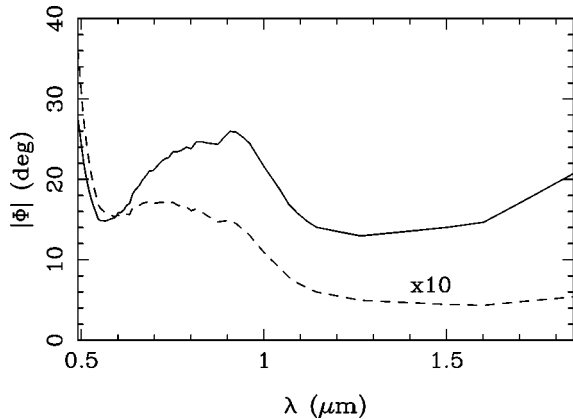
without constraint in the infinite planes parallel to the interfaces. However, correct interpretation must be sought in the quantum-mechanical theory, including the spin-orbit coupling.[16]

C. Bilayer Co/Au

We now discuss a bilayer made of 10 nm of Co covered by 50 nm of gold deposited on a glass substrate. For the TM mode, by addition of a small cobalt film thickness to the gold film, the mean reflectivity level as a function of the angle of incidence [Fig. 8(a)] decreases when compared to a Au film (Fig. 4). It reaches the Co level because the cobalt film is close to the substrate. We can see in Fig. 8(a) that the bilayer Co/Au has a plasmon resonance at 44.4° at the Au/air interface, which is similar to what we saw in Sec. IV A, where we had a Au film deposited on a glass substrate. A kind of Brewster angle appears as a minimum around 70° for the reflectivity curve in Fig. 8(a) for the TM mode. It could also appear if we increased the gold film thickness. The plasmon resonance is therefore softened. In the polar magnetization, for the TM mode [Fig. 8(b)], the Kerr curves also display this gold plasmon resonance as a significant peak at 44.4°. For this polarization, the plasmon resonance also appears as a peak at 633 nm in the Kerr rotation module as a function of the incident wavelength [Fig. 9(a)] because gold has a deep plasmon resonance at the Au/air interface.

For the TE mode, nothing special appears in the reflectivity curve except the classical increase as a function of the angle of incidence while the Kerr rotation module curve displays a dip for the critical angle at 41.8°, as we saw earlier for a single cobalt film [Fig. 8(b)]. Indeed, if we carefully observe both reflectivity and Kerr rotation module curves for the TE mode in the polar magnetization, we can conclude that the dip corresponding to the Kerr rotation curve as a function of the incident angle does not correspond to a plasmon resonance. This can be explained by the fact that both reflectivity and Kerr rotation curves as a function of the incident wavelength do not show the plasmon resonance at 633 nm, such as the TM mode shows [Figs. 8(a) and 9(a)].

For the longitudinal magnetization, in the TM mode, we see the plasmon resonance of Au as a peak in the Kerr rota-
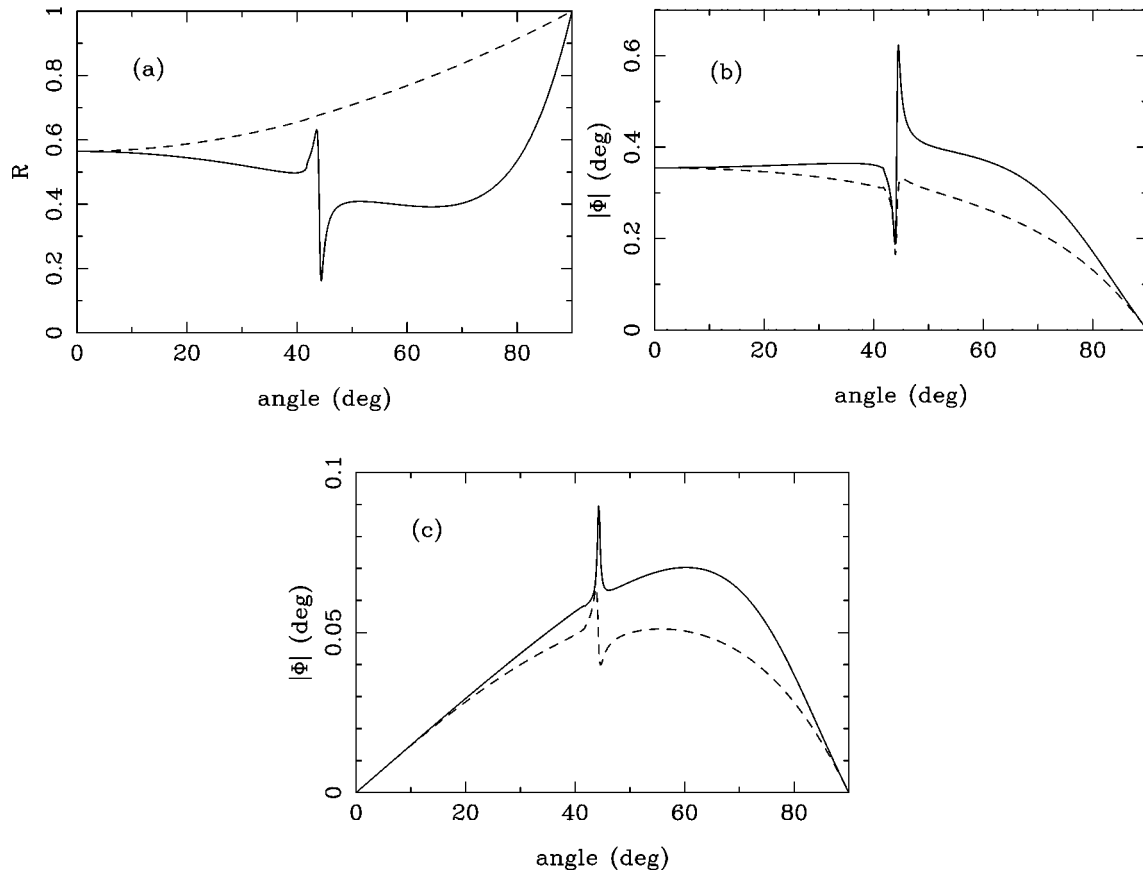

FIG. 7. For the same system as in Fig. 6, and for a $\theta = 51°$ variation of the Kerr rotation module $|\Phi|$ for the TM mode as a function of the incident wavelength for the polar magnetization (solid line) and the longitudinal magnetization (magnified ten times; dashed line).

FIG. 8. For λ = 0.633 μm, (a) reflectivity for both TE (dashed line) and TM (solid line) modes as a function of the angle of incidence of a 10-nm-thick Co film covered by a 50-nm-thick Au film on a glass substrate; (b) variation of the Kerr rotation module |Φ| for the TE (dashed line) and TM (solid line) modes as a function of the incident angle for the polar magnetization; (c) variation of the Kerr rotation module |Φ| for the TE (dashed line) and TM (solid line) modes as a function of the incident angle for the longitudinal magnetization.

tion module as a function of the angle of incidence [Fig. 8(c)], and also in the spectrum at 633 nm [Fig. 9(b)]. On the other hand, the TE mode shows a peak followed immediately by a dip, corresponding to the plasmon resonance at 44.4° in the Kerr rotation curve as a function of the angle of incidence [Fig. 8(c)]. The plasmon is well identified at 633 nm in the spectrum of Fig. 9(b). However, for this magnetization,

we see the plasmon resonance in the Kerr rotation module not only in the TM mode, but also in the TE mode. The plasmon resonance gives rise to a simply shaped peak in the TM mode. In the TE mode, the peak has quite a different structure, not only as a function of the angle of incidence but also as a function of the wavelength. Basically, it looks like the spectral response of a damped oscillator. Thus the direc-
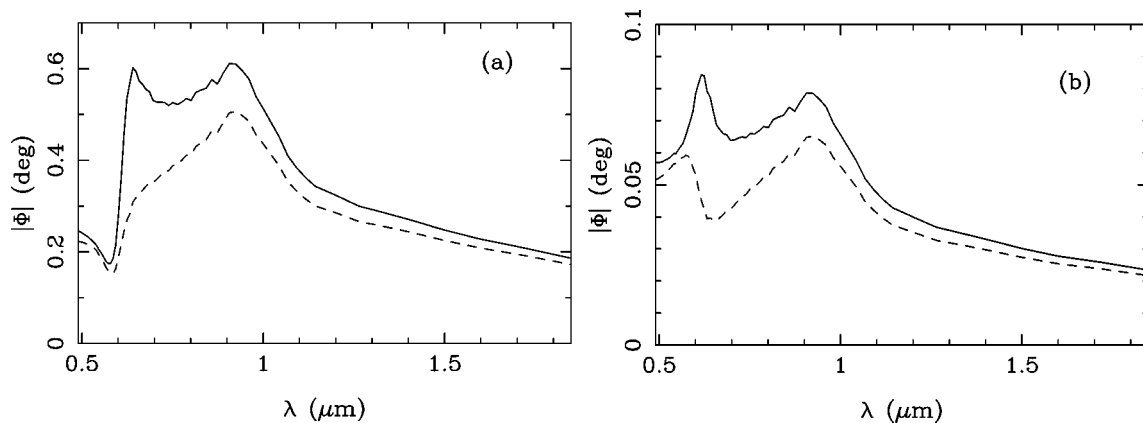

FIG. 9. For the same system as in Fig. 8, and for a θ = 44.4° (a) variation of the Kerr rotation module |Φ| for the TE (dashed line) and TM (solid line) modes as a function of the incident wavelength for the polar magnetization; (b) variation of the Kerr rotation module |Φ| for the TE (dashed line) and TM (solid line) modes as a function of the incident wavelength for the longitudinal magnetization.
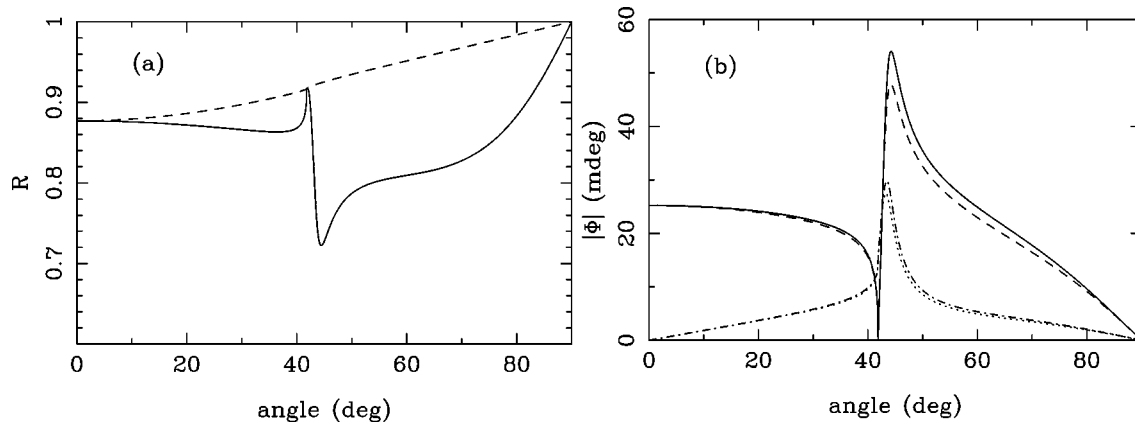
FIG. 10. For $\lambda = 0.633$ μm, (a) reflectivity for both TE (dashed line) and TM (solid line) modes as a function of the angle of incidence of a 50-nm-thick Au film covered by a 10-nm-thick Co film on a glass substrate; (b) variation of the Kerr rotation module $|\Phi|$ for the TE (dashed line) and TM (solid line) modes for the polar magnetization, and for the TE (dotted line) and TM (dotted-dashed line) modes for the longitudinal magnetization (magnified three times), as a function of the incident angle.

tion of the applied static magnetic field is very important in a study of the Kerr rotation under the condition of plasmon resonance [see Figs. 8(c) and 9(b)].

For the TE mode, it is very important to notice that, in the longitudinal case, a z component appears in the scattered field which was absent in the incident electric field. This is due to the form of the dielectric tensor (52), and particularly to the element ε_{13}. This scattered field excites the plasmon resonance at the gold/air interface. This cannot occur in the TE mode for the polar magnetization because, in this case, only components parallel to the interfaces are created, and they cannot excite a plasmon resonance at the gold/air interface.

Thus the optical effects related to the plasmon resonance appear in the spectrum between 550 and 700 nm, whereas the peak centered on 950 nm has a different origin (Fig. 5): it corresponds to the spin-orbital effects of the Co layer, and especially to the extremal values of the nondiagonal elements which appear in the dielectric tensors of Co [Eqs. (51) and (52)]. The influence of the maximum absolute value of Re β (see Fig. 3) is found in all Kerr spectra as a broad peak between 900 and 1000 nm. This broad peak is not related to any optical or plasmon effect. Peaks occurring between 500 and 800 nm are thus attributed to optical or plasmon effects of thin films.

D. Bilayer Au/Co

We set 50 nm of Au covered by 10 nm of Co deposited on a glass substrate. By addition of a small cobalt thickness to the gold film, the reflectivity level is close to that of a single Au film deposited on a glass substrate [Fig. 10(a)].

For the TM mode, the plasmon resonance still exists, and takes place at the Co/air interface; it appears as a minimum in the reflectivity curve at 44.4° in Fig. 10(a). For the TM mode, the dip in the reflectivity curve as a function of the angle of incidence corresponding to the plasmon resonance is larger for a thin cobalt film as compared to a gold one. This is due to the greater absorption of the cobalt film.

The plasmon resonance occurs at the same angle for the Co/Au system and also for the Au/Co system for the TM

mode. For the Au/Co system, the plasmon resonance must be the same as that of the Co/air interface, which should appear around 51° in the reflectivity curve as a function of the angle of incidence. The shift of this angle to 44.4° is due to the presence of the Au film.

We can see, at first, that the intensity range of the Kerr curves [cf. Fig. 10(b)] is smaller than in the bilayer studied previously. This is due to the absorption, not only of Co but also of Au. Indeed, the optical field is already drastically reduced when reaching the anisotropic Co film. For the polar magnetization, the critical angle appears as a significant dip on the Kerr rotation curve as a function of the angle of incidence [Fig. 10(b)]. For all magnetizations and all incident optical polarization modes, the plasmon resonance arises in the Kerr rotation module as a function of the angle of incidence [Fig. 10(b)].

V. CONCLUSION

Using a numerical application of Green's dyadic technique, the Kerr rotation spectra have been carefully studied beyond the critical angle for total reflection . Particularly, the excitation of surface plasmons in Au/Co bilayers by a TE incident field has been shown to be due to the anisotropic dielectric tensor of magneto-optical materials. In the spectrum of the Kerr rotations, this study brings to the fore the difference between the plasmon effects which appear between 550 and 700 nm, and the spin effects which appear between 800 nm and 1 μm. This has some importance in the interpretation of the Kerr rotation measurements.

[1] S. D. Bader and J. L. Erskine, in *Ultrathin Magnetic Structures*, edited by J. A. C. Bland and B. Heinrich (Springer-Verlag, Berlin, 1994), Vol. 2.

[2] H. Ebert and G. Schütz, *Spin-Orbit-Influenced Spectroscopies of Magnetic Solids* (Springer-Verlag, Berlin, 1996).

[3] J. Zak, E. R. Moog, C. Liu, and S. D. Bader, J. Magn. Magn. Mater. **89**, 107 (1990).

[4] J. Zak, E. R. Moog, C. Liu, and S. D. Bader, J. Magn. Magn. Mater. **88**, L261 (1990).

[5] H. Takeshita, T. Katayama, and A. Itoh, Appl. Phys. Lett. **68**, 3040 (1996).

[6] M. Hayashi and T. Katayama, J. Magn. Magn. Mater. **126**, 547 (1993).

[7] W. Geerts, T. Katayama, and Y. Suzuki, J. Magn. Soc. Jpn. **19**, 309 (1994).

[8] W. Geerts, T. Katayama, and Y. Suzuki, Phys. Rev. B **50**, 12 581 (1994).

[9] V. I. Safarov *et al.*, Phys. Rev. Lett. **73**, 3584 (1994).

[10] C. Girard and A. Dereux, Rep. Prog. Phys. **59**, 657 (1996).

[11] A. A. Maradudin and D. L. Mills, Phys. Rev. B **11**, 1392 (1975).

[12] A. Yaghjian, Proc. IEEE **68**, 248 (1980).

[13] E. D. Palik, in *Handbook of Optical Constants of Solids*, edited by E. D. Palik (Academic, New York, 1991).

[14] G. S. Krinchik and V. A. Artem'ev, Sov. Phys. JETP **26**, 1080 (1968).

[15] H. Raether, *Surface Plasmons on Smooth and Rough Surfaces and on Gratings* (Springer, Berlin, 1988).

[16] P. N. Argyres, Phys. Rev. **97**, 334 (1955).